REMARKS/ARGUMENTS

Favorable reconsideration of this application in light of the following discussion is respectfully requested.

Claims 1-7, 9-11, 14-27, 29-31, 34-40 and 44-46 are presently active. Claims 8, 12-13, 28, and 32-33 have been presently canceled without prejudice. Claims 1, 21, and 44 have been presently amended.

Applicant acknowledges with appreciation the consideration of this matter and the related appeals in U.S. Serial Nos. 10/673,467; 10/673,501; 10/673,506; and 10/673,583 by the Board.

Claim 1 as clarified defines:

> 1. A method of facilitating a process performed by a semiconductor processing tool, comprising:
>   inputting a first principles physical model including a set of computer-encoded differential equations, the first principles physical model describing at least one of a basic physical or chemical attribute of the semiconductor processing tool;
>   inputting process data related to an actual process being performed by the semiconductor processing tool;
>   setting initial and boundary conditions *for a spatially resolved model of a physical geometry of the semiconductor processing tool* based on said process data related to the actual process being performed by the semiconductor processing tool;
>   solving the computer-encoded differential equations of the first principles simulation model *for the spatially resolved model concurrently with the actual process being performed and in a time frame shorter in time than the actual process being performed*;
>   providing a first principles simulation result from the solution of the computer-encoded differential equations solved concurrently with the actual process being performed; and
>   using the first principles simulation result obtained during the performance of the actual process to facilitate the actual process being performed by the semiconductor processing tool. [Emphasis added.]

Applicant's specification at numbered paragraph [0035] states:

> Thus, the first principles physical model 106 depends to some extent on the type of semiconductor processing tool 102 analyzed as well as the process performed in the tool. For example, *the physical model 106 may include a spatially resolved model of the physical geometry of the tool 102,*

which is different, for example, for a chemical vapor deposition (CVD) chamber and a diffusion furnace. Similarly, the first principles equations necessary to compute flow fields are quite different than those necessary to compute temperature fields. The *physical model 106 may be a model as implemented in commercially available software, such as ANSYS, of ANSYS Inc., Southpointe, 275 Technology Drive Canonsburg, PA 15317, FLUENT, of Fluent Inc., 10 Cavendish Ct. Centerra Park, Lebanon, NH 03766, or CFD-ACE+, of CFD Research Corp., 215 Wynn Dr., Huntsville, AL 35805, to compute flow fields, electro-magnetic fields, temperature fields, chemistry, surface chemistry (i.e. etch surface chemistry or deposition surface chemistry).*

One of ordinary skill in the art would know that a "spatially resolved model of a physical geometry of the semiconductor processing tool" is simply a model of the physical geometry of the tool using separated points in space.

Applicant's specification at numbered paragraph [0091] describes a number of process sensors detecting for example mass flow rates, chamber pressure, temperatures of the substrate holder and the substrate, a temperature of a backside gas coolant, gas gap pressure, and vacuum pump inlet pressure. Thereafter, Applicant's specification at numbered paragraph [0092] states:

> A diagnostic controller **1324** can be coupled to each of the *sensors* described above *and can be configured to provide measurements from these sensors to the simulation module described above*. For the exemplary system of FIG. 13, the model executed on the simulation module can, for example, include three components, namely, a thermal component, a gas dynamic component, and a chemistry component. In the first component, the gas-gap pressure field can be determined, followed by a calculation of the gas-gap thermal conductance. Thereafter, the *spatially resolved temperature field* for the substrate (and substrate holder) can be determined by *properly setting boundary conditions (and internal conditions)* such as *boundary temperature, or boundary heat flux, power deposited in resistance heating elements, power removed in cooling elements, heat flux at substrate surface due to the presence of plasma,* etc. [Emphasis added]

Applicant's specification at numbered paragraph [0057], states:

> In this embodiment, steady-state simulations are repeatedly run concurrently with the process by using the physical sensor measurements to repeatedly update boundary conditions of the first principles simulation model.

Hence, Applicant discloses 1) a physical model 106 including a spatially resolved model of the physical geometry of the tool 102, 2) physical model 106 implemented in commercially available software such as ANSYS or FLUENT to solve a spatially resolved model, 3) the setting of boundary and internal conditions, 4) repeated running of simulations concurrently with the process, and 5) using physical sensor measurements to repeatedly update boundary conditions of the first principles simulation model.

The test of enablement is whether one reasonably skilled in the art could make or use the invention from the disclosures in the patent coupled with information known in the art without undue experimentation." United States v. Telectronics, Inc., 857 F.2d 778, 785 (Fed. Cir. 1988).

For the Examiner's consideration of what was known in the art at the time of filing,[1] attached is a 2002 article from *Chemical Engineering Science* entitled: "Visualization and numerical simulation of fine particle transport in a low-pressure parallel plate chemical vapor deposition reactor." This article on page 509 shows the use of spatially resolved model of the physical geometry of a parallel plate CVD reactor (i.e., set of 2,000,000 triangular/tetrahedral meshes). This article on page 499 indicates that the numerical simulations were performed using the commercially available CFD code Fluent 5.3 (Fluent, Inc.). Excerpts from this paper are reproduced below on the next page. While provided for the sake of showing that one of ordinary skill in the art would not have to use undue experimentation to make a spatially resolved model of a physical geometry of the semiconductor processing tool, this reference also does not show the use of solutions from such models being used for process control or being produced in a time frame consistent with that of a semiconductor manufacturing process.

---

[1] M.P.E.P. § 2164.05(a), the specification need not disclose what is well known to those skilled in the art and preferably omits that which is well known to those skilled and already available to the public.

14

Hence, given this knowledge in the art at the time of the invention, Applicants'

description of "setting initial and boundary conditions for a spatially resolved model of a

physical geometry of the semiconductor processing tool" does not require undue

experimentation and is enabled.

$$T_a = -1283.0\,r^2 - 84.658\,r + 361.79 \qquad T_c = -16802.0\,r^2 + 3835.2\,r + 282.06$$
$$T_b = -5678.8\,r^2 + 189.06\,r + 547.11 \qquad T_d = 62387.0\,z^2 - 992.5\,z + 385.15$$
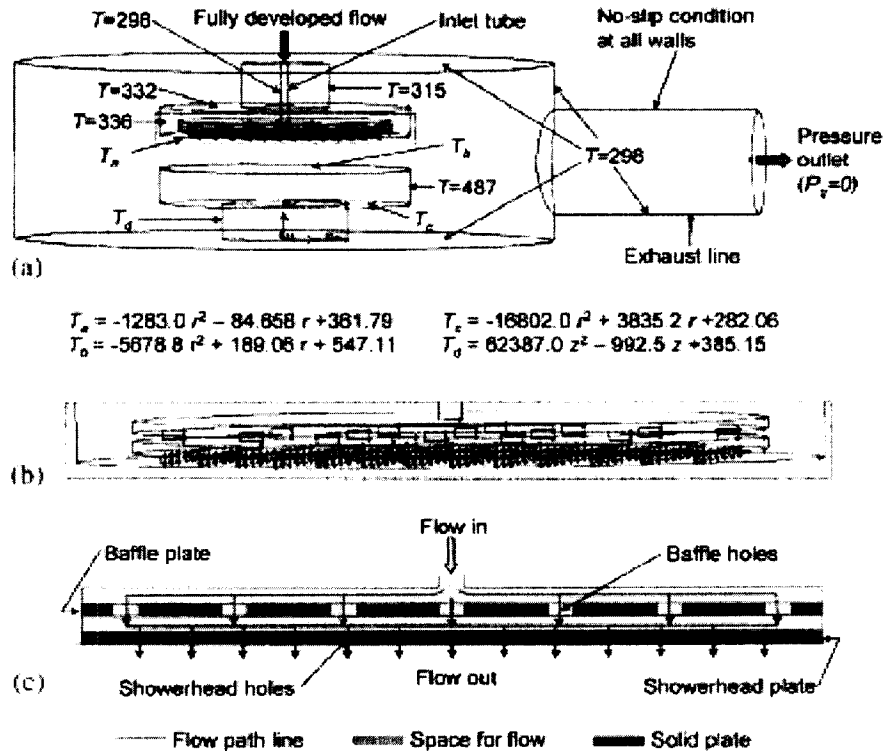
Fig. 3. (a) Computational domain and boundary conditions for the numerical simulation, (b) enlarged picture of the showerhead structure shown in (a), and (c) detail of the showerhead structure. The unit of temperature T shown in this figure is in K. r and z in the fitting equations of temperature profile represent radial and axial positions in m, respectively.

Total number of mesh nodes $\approx 2.0 \times 10^6$

Fig. 4. Unstructured triangular/tetrahedral grid arrangement used in the calculation.

15

Moreover, "solving the computer-encoded differential equations of the first principles

simulation model for the spatially resolved model concurrently with the actual process being

performed and in a time frame shorter in time than the actual process being performed," is

enabled as noted in the previously filed Appeal Brief:

> The examiner requested details of the models which lead to the unexpected result of being able to avoid the lengthy time conventionally required for the generation of a first principles model simulation. See page 10 of the Office Action. Appellant points out procedures by which the unexpected results of the invention are achieved. It is not the details of the models, but rather the details as to how the model calculations are implemented which reduce the time for calculations. For instance, the disclosed characteristics in the specification which permit simulation results to be obtained in a time frame compatible with using the first principles model simulation result for real time process control are enumerated below with reference to the numbered paragraphs in the filed specification:
>
> > 1) the use of interconnected resources inside a semiconductor device manufacturing facility to perform the first principles simulation (see specification, numbered paragraph [0043] and Figure 3, both reproduced below),
> >
> > 2) the use of code parallelization among interconnected computational resources inside the semiconductor device manufacturing facility (see specification, numbered paragraphs [0047] and [0048] reproduced below),
> >
> > 3) the sharing of simulation information among interconnected resources inside the semiconductor device manufacturing facility (see specification, numbered paragraphs [0047] and [0048] reproduced below), and
> >
> > 4) the reduction in redundant execution of substantially similar first principles simulations by the reuse of known solutions as initial conditions for the first principles simulation, as features which used singularly or in combination lead to a simulation result in a time frame consistent with real time process control in a semiconductor processing tool (see specification, numbered paragraphs [0047] and [0048] reproduced below).

Figure 3
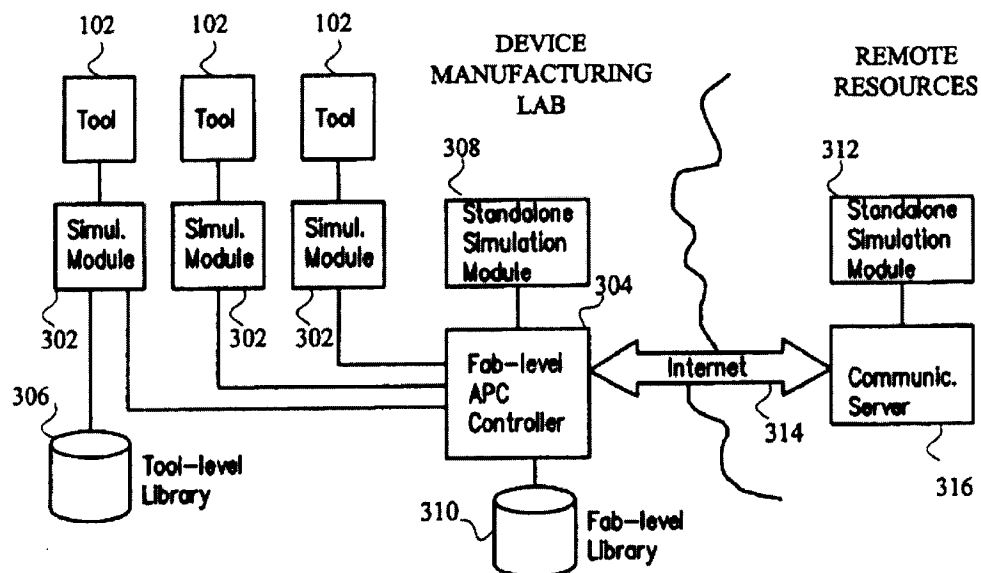
[0043] FIG. 3 is a block diagram of a network architecture that may be used to provide first principles simulation techniques to facilitate a process performed by a semiconductor processing tool in accordance with an embodiment of the present invention. As seen in this figure, the network architecture includes a device manufacturing fab connected to remote resources via the Internet 314. The device manufacturing fab includes a plurality of semiconductor processing tools 102 connected to respective simulation modules 302. As described with respect to FIG. 1, each semiconductor processing tool 102 is a tool for performing a process related to manufacturing a semiconductor device such as an integrated circuit. Each simulation module 302 is a computer, workstation, or other processing device capable of executing first principles simulation techniques to facilitate a process performed by a semiconductor processing tool 102. Thus, each simulation module 302 includes the first principles physical model 106 and the first principles simulation processor 108 described with respect to FIG. 1, as well as any other hardware and/or software that may be helpful for executing first principles simulations. Moreover, simulation modules 302 are configured to communicate with the fab-level advanced process control (APC) controller using any known network communication protocol. Each simulation module 302 may be implemented as a general purpose computer such as the computer system 1401 of FIG. 14.

[0047] The present inventors have discovered that the network configuration of FIG. 3 provides computational and storage resource sharing that allows a broad range of first principles simulation results at reasonable solution speeds, thus providing meaningful on-tool simulation capabilities that can facilitate processes performed by the tool. Specifically, while simple simulations may be executed by a tool's dedicated simulation module, complex simulations requiring greater computational resources may be executed using code parallelization techniques on multiple simulation modules in the network that may be on-tool or standalone. Even on-tool simulation modules in equipment currently under preventive maintenance may be used as a shared computational resource, provided there is power to the simulation module. Similarly, simulation results used for later lookup can be stored in libraries (e.g. storage devices) anywhere in the fab network, and accessed by all tools when lookups of diagnostic or control data are made.

[0048] The present inventors have also discovered that the network architecture of FIG. 3 provides the ability to distribute model results done at one processing tool 102 for one condition set, to other similar or identical tools operating later under the same or similar conditions, so redundant simulations are eliminated. Running simulations only for unique processing conditions at on-tool and standalone modules and re-using results from similar tools that have already known simulated solutions allows for rapid development of lookup libraries containing results that can be used for diagnostics and control over a large range of processing conditions. Further, the reuse of the known solutions as initial conditions for first principles simulation reduces the computational requirements and facilitates the production of simulated solutions in a time frame consistent with on-line control. Similarly, the network architecture of FIG. 3 also provides the ability to propagate changes and refinements made to physical models and model input parameters from one simulation module to others in the network. For example, if during process runs and parallel executions of a model it is determined that some input parameters need to be changed, then these changes can be propagated to all other simulation modules and tools via the network.

Hence, the examiner should now understand as before (when the former 112, first

paragraph, rejections were removed based on this information) that it is the combination of

one or more of the network architecture of FIG. 3, the sharing of model results done for one

condition set to other similar or identical tools operating later under the same or similar conditions, the reuse of prior solutions of proven convergence, the reuse of the known solutions as initial conditions for first principles simulation, etc. and **not the details of the model itself** which enable the invention to solve the computer-encoded differential equations of the first principles simulation model for the spatially resolved model concurrently with the actual process being performed and in a time frame shorter in time than the actual process being performed.

These capabilities taught by Applicant's specification permits for the remarkable control of semiconductor manufacturing processes using real time simulation results to control the process.

For example, the examiner will appreciate that, for the parallel plate reactor of Figure 13, a spatially resolved model of the parallel plate reactor and substrate on a stage opposing a plasma heat flux can be provided with the commercially available software, such as ANSYS or FLUENT packages discussed above. The disclosed sensors at numbered paragraph [0091] can provide temperature data of the substrate holder, the substrate, and the backside gas coolant during the process. This process data along with the above-noted properly set "boundary conditions (and internal conditions) such as boundary temperature, or boundary heat flux, power deposited in resistance heating elements, power removed in cooling elements, heat flux at substrate surface due to the presence of plasma, etc." can be used to set the initial and/or boundary conditions of the spatially resolved model.

The simulation then provides for example a spatial mapping of the heat flux to the substrate by taking into consideration heat flux from the plasma to other surfaces of the parallel plate reactor besides the substrate. The spatial mapping of the heat flux to the substrate becomes a simulation result, which can then be used to control the parallel plate reactor.

If the spatial map shows deviations outside the desired uniformity, then the process pressure or the gas composition could be changed while the process is running. With the invention having the capability to solve the computer-encoded differential equations of the first principles simulation model for the spatially resolved model in a time frame shorter in time than the actual process being performed, this simulation tool can simulate the effects of pressure and gas composition changes before actually having to implement the change.

This results in a remarkable advance in process control.

Regarding the art of record, Applicants submit that this rejection should be removed for the following reasons.

Firstly, Claim 1 as clarified recites:

> setting initial and boundary conditions for a spatially resolved model of a physical geometry of the semiconductor processing tool based on said process data related to the actual process being performed by the semiconductor processing tool.

M.P.E.P. § 2142.02 indicates that:

> In determining the differences between the prior art and the claims, the question under 35 U.S.C. 103 is not whether the differences themselves would have been obvious, but whether the claimed invention as a whole would have been obvious.

The art of record in this application or the related appealed applications noted above neither individually nor in combination discloses or suggests setting initial and boundary conditions for a spatially resolved model of a physical geometry of the semiconductor processing tool.

The examiner in related application U.S. Serial No. 10/673,507 relied on col. 7, lines 21-35, of Sonderman et al for an asserted teaching of setting initial and boundary conditions

for a spatially resolved model of a physical geometry of the semiconductor processing tool.

Yet, col. 7, lines 21-35, of <u>Sonderman et al</u> merely describes:

> Turning now to FIG. 5, a flowchart representation of the steps for performing the process simulation function described in block 440 of FIG. 4, is illustrated. The system 100 prepares one or more process models for simulation (block 510). The models that are prepared for simulation may include the device physics model 310, the process model 320, and the equipment model 330. The number of models defined by the system 100 generally depends upon the interactions of model-components that are to be examined by the simulator 340. In other words, the system 100 determines which components in a model are to be modified and which components are to be monitored for reactions caused by the original component modification. One embodiment of a flowchart depiction of the steps of preparing the processing models for simulation is illustrated in FIG. 6

There is no detail here of a spatially resolved model of a physical geometry of the semiconductor processing tool or the setting initial and boundary conditions for a spatially resolved model of a physical geometry of the semiconductor processing tool.

The greatest detail of the equipment model provided by <u>Sonderman et al</u> is at col. 5, lines 62-67, which states:

> The equipment model 330 comprises components that can model furnace behavior during semiconductor manufacturing processes. The equipment model 330 can also model the temperature response, pressure response, and at other such characteristics relating to equipment that performs manufacturing processing.

There is once again no detail here of a spatially resolved model of a physical geometry of the semiconductor processing tool or the setting initial and boundary conditions for a spatially resolved model of a physical geometry of the semiconductor processing tool.

Moreover, statistical models, like <u>Sonderman et al</u> (and <u>Tan et al</u>), do **not** have initial and boundary conditions, but rather are models which simply correlate inputs and outputs of a process based on statistical data from previous process runs. These models also do not solve for a variable over a gridded spatial domain, but instead use statistics to provide predictions about the end result that would be obtained if a process were run in a certain manner.

21

Indeed, the one model described in detail in <u>Sonderman et al</u> is their device physics

model, which is set forth at col. 9 of <u>Sonderman et al</u>. This "model" is based on performance

factors X_{Ai} fed back into line 805, through which a learned model is developed based on the

system performance over time. Col. 9, lines 1-11, state:

> Turning now to FIG. 8 , a simplified process control system block diagram is illustrated. The controller 810 controls a process 820 that is performed on a silicon wafer. The input to the controller on a line 805 , is denoted by the term $X_{Ti,}$ which represents a target performance of the processed semiconductor wafer (S_i). Once a particular silicon wafer, S_i, is processed, metrology results 830 will define the actual performance of the processed semiconductor wafer S_i, which is denoted by the term X_{Ai}. The actual performance factor, X_{Ai} is *fed back* into the line 805 which is sent to the controller for further adjustments.

<u>Sonderman et al</u> further describe at col. 9, lines 33-40, how the percentage

effectiveness (i.e., a statistical metric) is derived based on a multi-variant function (i.e..,

another statistical metric).

Hence, the statistical models in <u>Sonderman et al</u> would be of no consequence to initial

and boundary conditions for a spatially resolved model of a physical geometry of the

semiconductor processing tool.

Furthermore, while the examiner in related application U.S. Serial No. 10/673,507

relied on col. 3, lines 50-67, and col. 7, lines 8-20 of <u>Sonderman et al</u> for an asserted teaching

of inputting process data for an actual process being performed by the semiconductor

processing tool, those section of <u>Sonderman et al</u> only state:

> **Col. 3, lines 50-57:** Semiconductor devices are processed in a manufacturing environment using a number of input control parameters. Turning now to FIG. 1, a system 100 in accordance with one embodiment of the present invention is illustrated. The system 100 comprises a process control environment 180, a manufacturing/processing environment 170, and a simulation environment 210. The process control environment 180 controls the operations of the manufacturing environment 170. In one embodiment, the process control environment comprises an APC framework. *The process control environment 180 can receive data from the manufacturing environment 170 and the simulation environment 210* and make appropriate

changes to manufacturing control parameters to affect the operations of the manufacturing environment 170.

In one embodiment, semiconductor devices 105, such as semiconductor wafers, are processed on processing tools 120a, 120b using a plurality of control input signals, or manufacturing parameters, on a line 123.

Col. 7, lines 8-20: Once the system 100 validates the defined models, the system 100 acquires data to operate the defined models (block 630). In one embodiment, the system 100 acquires data from the computer system 130 in order to operate the defined models. The system 100 then populates the defined models with the data acquired by the system 100 for operation of the models (block 640). In other words, the system 100 sends operation data, control parameter data, simulation data, and the like, to the defined models so that the defined models can perform a simulation *as if an actual manufacturing process were being performed*. The completion of the steps described in FIG. 6 substantially completes the step of preparing process models for simulation, as indicated in block 510 of FIG. 5.

With regard to the first emphasized section above, that section states that "the process control environment 180 can receive data from the manufacturing environment 170," there is no indication that the received data is data for setting initial and boundary conditions for a spatially resolved model of a physical geometry of the semiconductor processing tool. The received data may well have been metrology data, which would have been data taken on a sample sent to the metrology tool 150.

Indeed, Sonderman et al specifically call out at col. 4, line 67, to col. 5, line 9, that the manufacturing environment 170 can send metrology data results into the simulation environment 210, and further state:

The simulation environment 210 can then use the metrology data results and perform various tests and calculations to provide more accurate, modified control parameters to the process control environment 180. A feedback loop in then completed when the process control environment 180 sends the modified or adjusted process control parameters to the manufacturing environment 170 for further processing of semiconductor wafers.

Metrology data would be of no consequence to initial and boundary conditions for a spatially resolved model of a physical geometry of the semiconductor processing tool.

With regard to the second emphasized section, the examiner will note that the description there is consistent with the statistical multi-variant description in <u>Sonderman et al</u> of their device model, discussed above, which also would be of no consequence to initial and boundary conditions for a spatially resolved model of a physical geometry of the semiconductor processing tool.

Thus, these passages relied on by the Examiner fail to disclose any indication of any process data being used to set initial and boundary conditions for a spatially resolved model of a physical geometry of the semiconductor processing tool.

Accordingly, <u>Sonderman et al</u> fail to disclose setting initial and boundary conditions for a spatially resolved model of a physical geometry of the semiconductor processing tool.

Secondly, the combination of <u>Sonderman et al</u> and <u>Jain et al</u> is improper because it is without a reasonable expectation of success and a person skilled in the art at the time of the invention would not have been motivated to risk control of a semiconductor processing unit to the unproven technology of <u>Jain et al</u>'s MPE.

The examiner has relied in the past on <u>Jain et al</u> for an asserted teaching of solving the computer-encoded differential equations of the first principles simulation model for the spatially resolved model. As previously noted, <u>Jain et al</u> describe at pages 372-373 that:

> We *propose* a wafer scale implementation of the MPE. The starting point would be a dedicated processing cell, optimized specifically for the PDE arithmetic and data routing. Because of the relative simplicity of the cell, it is expected that extremely large arrays (8x8 to 32x32) *could be* successfully processed on a single piece of silicon using Wafer Scale Integration techniques. In fact, we have already laid the foundation for the development of such a processing cell. Our Universal Multiply-Subtract-Add [11] *could be* adapted for this first cell design. Similarly, our nonlinear coprocessor cell [12]-[14] *might be used* in conjunction with the UMSA to provide advanced mathematical functions. As suggested in Fig. 2, there would be *courtyards of processors*, each with two interconnection networks and two memory banks. 2-D, 3-D, and 4-D problems could then be mapped for parallel computations. Since inter-processor delays are very small (say a few ns), extremely high speeds could be achieved. This, together with the high degree of parallelism,

would result also in high throughout. We *envision* 100 to 1000 processors (on one wafer) forming a wafer scale MPE. At a clock frequency of 50 MHz, a single wafer could achieve up to 20 GFLOPs performance. With our nonlinear coprocessor added, each instruction could equate to multiple floating point operations.

Furthermore, because of the extendible architecture, several wafers *could be* interconnected as shown in Fig. 5 to construct a "stacked" MPE wafer system (SMPE). Note that no vertical interconnects within the stack of wafers are expected. Tens to hundreds of GFLOPs performance in a volume the size of a desk-top computer [15] *could* thus be achieved. However, *these predictions* ignore the likely technical advances in the next five years; a tenfold further increase in performance *might be achievable*. [Emphasis Added]

Thus, as emphasized above, the proposed development work in Jain et al requires the

development of *futuristic* computational equipment which one of ordinary skill in the art

would be reluctant to implement or utilize for the rigorous standards needed in semiconductor

manufacturing.

Yet, the prior art can be modified or combined to reject claims as *prima facie* obvious

as long as there is a reasonable expectation of success. *In re Merck & Co., Inc.*, 800 F.2d

1091, 231 USPQ 375 (Fed. Cir. 1986). The Court in *Medichem S. A. v. Rolabo S. L.*, 437 F3d

1157, 77 USPQ2d 1865 (Fed. Cir. 2006) explained that:

> As stated above, an obviousness determination requires not only the existence of a motivation to combine elements from different prior art references, but also that a skilled artisan would have perceived a reasonable expectation of success in making the invention via that combination. While the definition of "reasonable expectation" is somewhat vague, our case law makes clear that it does not require a certainty of success. See In re O'Farrell, 853 F.2d 894, 903-04 (Fed. Cir. 1988) ("Obviousness does not require absolute predictability of success. . . . [A]ll that is required is a reasonable expectation of success.").
>
> However, to have a reasonable expectation of success, one must be motivated to do more than merely to "vary all parameters or try each of numerous possible choices until one possibly arrived at a successful result, where the prior art gave either no indication of which parameters were critical or no direction as to which of many possible choices is likely to be successful." Id. at 903. *Similarly, prior art fails to provide the requisite "reasonable expectation" of success where it teaches merely to pursue a "general approach that seemed to be a promising field of experimentation, where the prior art gave only general guidance as to the particular form of the claimed invention or how to achieve it."* Id. [Emphasis added.]

25

Here, Jain et al merely teach to pursue a general approach that seems to be a promising field of experimentation (i.e., the future obtainment of a sophisticated Mathematical Physical Engine MPE).

As attested to in the declaration filed in related application U.S. Serial No. 10/673,507, with the computing capability of Jain et al representing **futuristic, unrealized capability,** there is no reasonable expectation of success that computer-encoded differential equations of a first principles simulation model for a spatially resolved model of a semiconductor processing tool could have been solved in a time frame shorter in time than the actual process being performed in the semiconductor processing tool.

Accordingly, a person skilled in the art at the time of the invention would **not** have been motivated to risk control of a semiconductor processing unit to the unproven technology of Jain et al's MPE. Furthermore, a person skilled in the art at the time of the invention would **not** have had available to him Jain et al's MPE to use in a first principles simulation.

Hence, for these reasons, a combination of Sonderman et al and Jain et al is **not** proper.

Thirdly, Tan et al do not teach solving the computer-encoded differential equations of the first principles simulation model for the spatially resolved model concurrently with the actual process being performed and in a time frame shorter in time than the actual process being performed.

The examiner in related application U.S. Serial No. 10/673,507 relied on Tan et al for their teaching of at col. 2, lines 7-10, of model-based real time process control using in situ inputs, process models, and process control strategies to correctly process control parameters during the process run. Yet, a "model-based" real time process control does **not** specify when the model is completed, only that the "process control" in Tan is real time and does not

indicate that a solution to computer-encoded differential equations of the first principles

simulation model for a spatially resolved model of a physical geometry of the semiconductor

processing tool can be obtained in a time frame shorter in time than the actual process being

performed

Accordingly, Applicants resubmit that Tan et al do not disclose solving computer-

encoded differential equations of the first principles simulation model for a spatially resolved

model of a physical geometry of the semiconductor processing tool in a time frame shorter in

time than the actual process being performed.

Tan et al teach the use on an *existing* process model for feedback or feed forward

processing. In feedback control, by definition, the results of a process step are provided to a

subsequent wafer. In the feed forward control of Tan et al, the results of a prior process step

are used to adjust a subsequent process being run of the wafer. Tan et al describe:

> The illustrative APC Framework 200 includes a process model 202
> that receives *feed-forward and feed-back data* and calculates a processing
> parameter. The illustrative portion of the APC Framework 200 includes two
> measurement devices, in particular a pre-process metrology machine 204 and
> a post-processing metrology machine 206. The pre-process metrology
> machine 204 performs a measurement on a material prior to processing in a
> processing machine 208 and sends the measurement, as feed-forward data, to
> the process model 202. The processing machine 208 sends processed material
> to the post-processing metrology machine 206 *to measure post-process data
> which is sent to the process model 202 as feedback data*.

> Referring to FIG. 4, a schematic block diagram shows material flow of
> a processing step 400 of a semiconductor manufacturing process from a
> process engineer perspective. An APC plan 402 *retrieves a process model*
> from the data store 306, then executes a parameter calculation algorithm 404.
> The APC plan 402 gives the calculated parameters to a machine 406 and
> directs the machine 406 to execute the process. The machine 406 issues a
> signal to the APC plan 402 *when the process execution is complete*. The
> APC plan 402 sends the calculated parameters to the data history store 310 of
> the historical database 312.

> Referring to FIG. 5, a schematic block diagram shows material flow of
> a post-process measurement step 500 of a semiconductor manufacturing
> process from a process engineer perspective. An APC plan 502 sends a
> message to a machine 504 instructing the machine 504 to measure a post-
> processed material. The machine 504 sends measurement data to the APC

plan 502. The APC plan 502 retrieves an old process model from the data store 306. The APC plan 502 executes a model update algorithm 506. The APC plan 502 **stores an updated model in the data store 306 for usage in the processing step 400.** The APC plan 502 sends new model data to the data history store 310 of the historical database 312. [Emphasis added.]

Thus, <u>Tan et al</u> use post-process data to **update and store** a model for **a subsequent**

processing step. It is the **updated** model (completed ahead of the next run) that is used to

control the next process run, thereby providing the model-based real time process control

during the process run.

In other words, in <u>Tan et al</u>, the solution to the model exists **prior to process control is**

not derived concurrently with the process control.

Figure 2 of <u>Tan et al</u> (reproduced below) shows explicitly the use of "feed-forward

data" and "feed-back data" for process control modifications. Figure 3 of <u>Tan et al</u> shows

explicitly the use of "pre-process metrology" in what would be a feed-forward control

scheme. Figures 4 and 5 describe the use of an updated model to control a subsequent

process.

FIG. 2

28
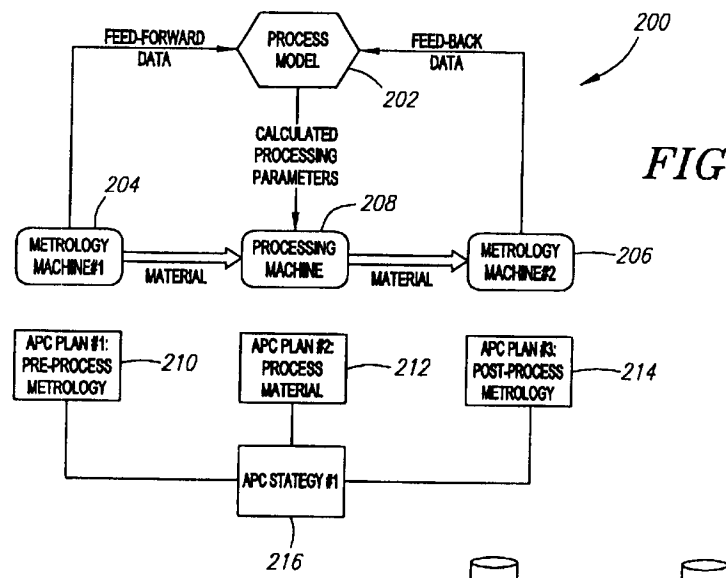
Figures 6-24 of Tan et al provide implementation details as to the processing described above.

Moreover, the previously filed declaration noted above attested to the fact that neither Sonderman et al nor Tan et al use a first principles simulation model. Rather, **as attested to**, the models in these references are 1) simplified models based on former approximate solutions or 2) statistical or "learned" models tracking how the systems are expected to behave.

Thus, even if the reading of the whole of Tan et al is discredited by the examiner, then the claim's recitation of *solving computer-encoded differential equations of the first principles simulation model* for a spatially resolved model of a physical geometry of the semiconductor processing tool is still **not** met because Tan et al do not use a first principles simulation model. In fact, as noted above, only Applicants have realized that computer-encoded differential equations of the first principles simulation model for a spatially resolved model of a physical geometry of the semiconductor processing tool can be solved in a time frame shorter in time than the actual process being performed.

Recent guidelines from the Patent Office regarding *KSR* published in Federal Register vol. 75, No. 169 (September 1, 2010) indicates at section five (5):

> 5. Federal Circuit Cases Discussing Consideration of Evidence. *Office personnel should consider all rebuttal evidence* that is timely presented by the applicants when reevaluating any obviousness determination. In the case of a claim rendered obvious by a combination of prior art references, applicants may submit evidence or argument to demonstrate that the results of the claimed combination were *unexpected*.
>
> Another area that has thus far remained consistent with pre- *KSR* precedent is the consideration of rebuttal evidence and secondary considerations in the determination of obviousness. As reflected in the MPEP, such evidence should not be considered simply for its "knockdown" value; rather, all evidence must be reweighed to determine whether the claims are nonobvious.
>
> Once the applicant has presented rebuttal evidence, Office personnel should reconsider any initial obviousness determination in view of the entire record. *See, e.g., In re Piasecki, 745 F.2d 1468, 1472, 223 USPQ 785, 788*

(Fed. Cir. 1984); In re Eli Lilly & Co., 90 F.2d 943, 945, 14 USPQ2d 1741, 1743 (Fed. Cir. 1990). All the rejections of record and proposed rejections and their bases should be reviewed to confirm their continued viability.

> MPEP § 2141.
> Office personnel should not evaluate rebuttal evidence for its "knockdown" value against the *prima facie* case, *Piasecki, 745 F.2d at 1473, 223 USPQ at 788,* or summarily dismiss it as not compelling or insufficient. If the evidence is deemed insufficient to rebut the *prima facie* case of obviousness, Office personnel should specifically set forth the facts and reasoning that justify this conclusion.

In *Ex parte Malone*, the Board reversed an obviousness decision reached by the examiner who had not considered the proffered evidence. *Ex parte Malone* stated:

> The Examiner's response to Nykerk Declaration is largely dismissive. In fact, even though Appellants' Briefs place extensive reliance on the Nykerk Declaration to overcome the prima facie case, the Examiner's Answer never addresses it in any detail. This is improper. Whether the claimed invention would have been obvious cannot be determined without considering evidence attempting to rebut the prima facie case. Manifestly, the Examiner's consideration and treatment of the Nykerk declaration is improper, since the Examiner has not reweighed the entire merits of the matter. Rather, he has dismissed the evidence of nonobviousness in a cursory manner. Since the Examiner did not properly consider the submitted evidence, the rejection cannot be sustained.

Support for Applicants position on this matter is also found in the following three references, previously supplied *as **rebuttal evidence***:

1) U.S. Pat. No. 6,185,472;
2) U.S. Pat. No. 7,047,095; and
3) U.S. Pat. No. 6,587,744.

The first reference describes a simulator that can be used "proceding semiconductor manufacturing processes" or for "correcting" predetermined schedules "without using testpieces." See col. 5, line 11-21. In other words, the simulator simulates process conditions and predicts outcomes based on the simulation such that optimized process recipes can then be used. In this aspect, U.S. Pat. No. 6,185,472 is similar to <u>Tan et al.</u>

The improvements in ab intio calculations described in U.S. Pat. No. 6,185,472 allow

a "prediction" of new process pathways by which semiconductor materials can be processed

(i.e., in future runs). Column 74 of U.S. Pat. No. 6,185,472 shows a reduction in processing

time from 15900 minutes to 159 minutes for the ab initio simulations. This timeframe of

over 2 hours for one simulation is too long and unworkable for real time process simulation

and control.

The second and third references describe feedback and feed forward process control

where the result of a simulation would not be obtained during the performance of the actual

process to control the actual process being performed, and therefore would not be used to

control the actual process performed by the semiconductor processing tool. In this aspect,

U.S. Pat. No. 7,047,095 and U.S. Pat. No. 6,587,744 are similar to Tan et al.

The second reference describes in the Summary Section:

In the system achieved in the first aspect or in the method achieved in
the second aspect, the control device may engage the transfer apparatus to
transfer the workpieces at least having undergone the processing executed by
the processing apparatus to the measuring apparatus, compare a measurement
value indicating the results of the processing having been executed on a
workpiece which is obtained through the measuring operation executed by the
measuring apparatus on the workpieces at least having undergone the
processing, with a target value for the processing results, and reset the
processing conditions for the processing apparatus in correspondence to an
error in the measurement value relative to the target value if the error is judged
to be equal to or greater than a specific value. It is to be noted that the
measuring operation may be executed on the workpiece before and after
undergoing the processing, instead of executing the measuring operation only
on the workpiece having undergone the processing.

The workpiece at least having undergone the processing executed by
the processing apparatus may be transferred by the transfer apparatus to the
measuring apparatus which then executes a measuring operation on the
workpiece at least having undergone the processing. The control device may
compare a measurement value indicating the results of the processing having
been executed on the workpiece obtained based upon the results of the
measuring operation by the measuring apparatus with a target value for the
processing results, observe the state of the fluctuation of an error in the
measurement value relative to the target value so as to predict the tendency of
the fluctuation and adjust the processing conditions for the processing

31

apparatus in correspondence to the tendency of the fluctuation error before the error exceeds a predetermined value. It is to be noted that in this case, too, the measuring operation may be executed on the workpiece before and after the processing instead of executing the measuring operation only on the workpiece having undergone the processing.

The third reference describes in the Abstract:

> A[n] automated run-to-run controller for controlling manufacturing processes comprises set of processing tools, a set of metrology tools for taking metrology measurements from the processing tools, and a supervising station for managing and controlling the processing tools. The supervising station comprises an interface for receiving metrology data from the metrology tools and a number of variable parameter tables, one for each of the processing tools, collectively associated with a manufacturing process recipe. The supervising station also includes one or more internal models which relate received metrology data to one or more variables for a processing tool, and which can modify variables stored in the variable parameter table to control the process tools using feedback and/or feed-forward control algorithms. Feed-forward control algorithms may, in certain embodiments, be used to adjust process targets for closed loop feedback control. The supervising station may have a user interface by which different feedback or feed-forward model formats (single or multi-variate) may be interactively selected based upon experimental or predicted behavior of the system, and may also permit users to utilize their own models for run-to-run control.

Thus, the only data of record with regard to a time frame for solving computer-encoded differential equations of a first principles simulation model is that given above of *over 2 hours*.

The Office has provided **no** evidence of any solution times **prior to the invention** for the solving of computer-encoded differential equations of a first principles simulation model for a spatially resolved model of a physical geometry of the semiconductor processing tool.

Fourthly, in support of Applicants' position on the non-obviousness of the claims, the filed declaration in related application U.S. Serial No. 10/673,507 attested to the fact that, prior to the filing of this application, a two-dimensional axisymmetric time-evolution temperature simulation of a chuck with a wafer, a plasma heat load, and a coolant heat removal was performed. By setting <u>initial and boundary</u> conditions *to values appropriate for*

the physical chuck setup, a time-evolving solution was obtained in less than 5 seconds, for a process of nominal duration of 60 seconds.

The model result expedited by the two-dimensional axisymmetric simplifications and the setting of initial and boundary conditions to values appropriate for the physical chuck setup.

The declaration attested to the fact that this simulation time gave a 12:1 factor time compression available for altering the controls to prevent running into "out-of-spec" process conditions, based on the prediction. This simulation result *in less than 5 seconds* occurred with all temperatures initialized to 0 deg C.

The declaration attested to the fact that, if an actual temperature at each time step from a previous wafer run had been used for initialization, the solver would not have had to make that many equilibrium iterations on each time step, even further shortening the time of solution.

As explained in the declaration in related application U.S. Serial No. 10/673,507, this result utilized a single core PC, with 1 GB of RAM (~2002), using ANSYS general-purpose simulation code, without any parallelization, and represented at the time *an unexpected result*.
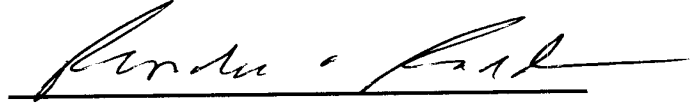
Hence, for all of these reasons given above, Claims 1-7, 9-11, 14-27, 29-31, 34-40 and 44-46 should be found non-obvious and passed to allowance.

Conclusion:

In view of the present amendment and in light of the above discussions, the

application as amended herewith is believed to be in condition for allowance.

Respectfully submitted,

OBLON, SPIVAK, McCLELLAND,
MAIER & NEUSTADT, P.C.

Customer Number

22850

Edwin D. Garlepp
Registration No. 45,330
Attorney of Record

Ronald A. Rudder, Ph.D.
Registration No. 45,618

Tel: (703) 413-3000
Fax: (703) 413 -2220
(OSMMN 08/03)
EDG:RAR:clh

34

Visualization and numerical simulation of fine particle transport in a low-pressure parallel plate chemical vapor deposition reactor

Heru Setyawan, Manabu Shimada, Kenji Ohtsuka, Kikuo Okuyama *

*Department of Chemical Engineering, Graduate School of Engineering, Hiroshima University, 1-4-1 Kagamiyama,
Higashi-Hiroshima 739-8527, Japan*

Abstract

The behavior of fine particles in a low-pressure parallel plate chemical vapor deposition reactor was investigated by constructing a system that permits particle motion in the reactor to be visualized. The test spherical silica aerosol particles, which were 1.0 μm in diameter and dispersed in argon gas, were fed into the reactor from the outside and particle motion was detected by a laser light scattering method. The effect of operating conditions, such as pressure and temperature, on particle transport in the reactor was investigated. The pressure was varied from 2.0 to 4.0 Torr and the wafer-substrate plate temperature was varied over the range of 25°C to 300°C. A three-dimensional numerical simulation was performed using the commercially available computational fluid dynamics code Fluent. A detailed configuration of the reactor, including the showerhead structure was considered when investigating this mechanism. It is found, both experimentally and by numerical simulation that, when the wafer-substrate plate is not heated, the effect of pressure on particle trajectory in the space between plates cannot be observed. However, at elevated temperature, i.e. when the wafer-substrate plate is heated, the particle trajectory is apparently influenced by pressure. In addition, the effect of thermophoresis, as the result of a temperature gradient by heating of the wafer-substrate plate is very pronounced for gas pressures of both 2.0 and 4.0 Torr. The experimentally observed phenomena were satisfactorily reproduced by simulation. © 2002 Elsevier Science Ltd. All rights reserved.

Keywords: CVD reactor; Particle contamination; Reduced pressure; Light scattering; Numerical simulation; Dynamic behavior

1. Introduction

Chemical vapor deposition (CVD) processes are commonly used to produce thin films in the microelectronics industry. Particle contamination becomes a major factor in these types of processes, since it causes severe problems during the production of the thin films. A major problem is pattern defects, which represent the main cause of yield reduction. Possible contamination sources include dirty gas lines, poor loading procedures, homogeneous gas phase nucleation, and flaking of the chamber surface material. Fine particles, which are generated during the deposition processes, represent one of the leading causes of defects and reduced yields, and because of this, the focus of particle contamination control in the microelectronics industry is increasingly shifting from the clean room environment

to the process tools themselves (Okuyama, Huang, Seinfield, Tani, & Kousaka, 1991; Okuyama, Huang, Seinfield, Tani, & Matsui, 1992; Rao et al., 1998). Thus, preventing particle generation during the deposition process is an issue of major importance. However, it is very difficult or even impossible to completely eliminate particle generation in such a process. Hence, controlling particle transport in the reactor in such a way so that the particles are deposited on surfaces other than the substrate is important. This is possible if we have a better understanding of the dynamics of particles in a fluid. Therefore, it is indispensable to develop a better physical understanding of the nature of fine particle transport in CVD reactors in order to eliminate contamination in the process equipment. In addition, product requirements are pushing the semiconductor industry in the direction of low-pressure processes (Choi, Rader, & Geller, 1996). Consequently, it is also important to understand particle transport under low-pressure operating conditions, since particle behavior under these conditions can be significantly different from higher-pressure processes.

* Corresponding author. Tel.: +81-824-24-7716; fax: +81-824-24-7850.

E-mail address: okuyama@hiroshima-u.ac.jp (K. Okuyama).

A parallel-plate type reactor is one of the widely used reactors in CVD processes. Particle transport in the reactor may be governed by a variety of mechanisms, including convection, diffusion, external forces and inertia (Adachi & Okuyama, 1998). Particle diffusion is important for small particles and/or at low pressure. Particle inertia is responsible for the deviation of the particle trajectories from the gas streamlines in the space between the plates. Schmidt, Fissan, and Schmidt (1996) showed that inertia has a strong effect on particle deposition in cases where small distances exist between the particle point injection and a surface. External forces can include gravity, electrical and thermophoresis. Gravity is an important force for the case of larger particles. In the large-particle limit, gravity becomes the dominating deposition mechanism (Choi et al., 1996; Garrity, Peterson, Garret, & O'Hanlon, 1995). Electric forces play an important role in dictating the transport of charged particles in the presence of electric field, such as in plasma processing tools. Thermophoresis may be significant in the presence of temperature gradients and plays an important role in particle deposition on semiconductor wafers (MacGibbon, Busnaina, & Fardi, 1999; Oh, Yoo, & Myong, 1996; Ye et al., 1991). The above workers showed that particle deposition could be reduced by increasing the temperature gradient between the wafer and walls including the showerhead. In addition, thermophoretic force also plays an important role in particle transport during the postplasma regime and keeps the particles moving away from the wafer (Collins, Brown, O'Hanlon, & Charlie, 1995).

There are two fundamentally different approaches for calculating particle transport dispersed in a gas flow in a parallel-plate reactor, and are referred to as the Lagrangian (Garrity et al., 1995; Choi et al., 1996) and Eulerian (Nijhawan, McMurry, & Campbell, 2000; Oh et al., 1996) methods. In the Lagrangian method, the particle force balance is integrated numerically along particle trajectories to give a particle velocity field. In the Eulerian method, the particle equations are solved in Eulerian form. This method allows similar techniques to be used both for a gas flow field and for particle trajectories. However, as pointed out by Slater and Young (2001), this method has difficulties relative to the implementation of particle boundary conditions at solid surfaces because the Eulerian equations cannot simultaneously convey information in two or more directions. This suggests that such a method cannot represent any degree of particle reflection. In addition, this method will experience ill-posed when individual particle pathlines cross, since in the particle equations, information can only travel through the computational domain in the direction of the particle pathlines.

All reported studies concerned with particle transport in a parallel plate CVD reactor have analyzed the particle transport mechanisms using a simplified reactor geometry. The gas flow in the space between plates was treated as the stagnation point flow. The results were then characterized in terms of collection efficiency. The agreement between the

spatial distribution of the number concentration of particles or the particle trajectories does not become an important issue as long as the collection efficiency is in good agreement (Nijhawan et al., 2000). There is no study which has addressed the issue of particle behavior in such a reactor by taking into account details of reactor configuration such as showerhead, baffle, and related items. In order to properly control particle contamination, details of the fluid flow in a given reactor configuration should be considered since the behavior of the particles is strongly dependent on the fluid flow field. In addition, there is no reported study in which the particle trajectories obtained from numerical simulation are compared to those from particle visualization experiments.

In this present work, we wish to report on a study of the behavior of fine particles in a low-pressure parallel plate-type CVD reactor by taking into account the details of reactor configuration, as well as of fluid flow. The role of thermophoretic force was investigated in detail, since it is one of the most important forces that influence fine particle movement in such a reactor. An experimental method to measure particle transport and behavior in the reactor was developed. In this case, inert particles injected from outside into the low-pressure reactor were used so that the particle size could be well defined. A system was developed to deliver particles from a higher-pressure environment to a low-pressure chamber for the purpose of visualization. The particle trajectories in the space between the plates were observed by using a laser light scattering (LLS) technique. A three-dimensional numerical simulation using computational fluid dynamics (CFD) was carried out, in order to elucidate the mechanism of particle transport.

2. Experimental technique and apparatus

Fig. 1 shows a schematic diagram of the experimental apparatus. The main equipment consists of (i) an aerosol generator equipped with pressure reduction system, (ii) a conventional parallel plate-type reactor, and (iii) an LLS system to visualize particle motion. The dimension and configuration of the reactor have been reported elsewhere (Fujimoto et al., 2000). Briefly, the upper plate is a showerhead where gas enters the reactor. It has 145 holes with diameter of 1.0 mm. A baffle that contains 16 holes with diameter of 6.0 mm is installed above the showerhead. The wafer-substrate plate is the position where the substrate being processed is placed, and the temperature is controlled by a controller.

Test spherical silica particles 1.0 μm in diameter were dispersed into argon gas by an aerosol generator (RBG-1000, Tokyo Dylec) prior to feeding into the reactor. The problem encountered in delivering particles from atmospheric pressure into a very low-pressure environment is a tendency of the capillary pressure reducer to be clogged by particles. If this occurs, the continuous supply of particles for the purpose of visualization cannot be guaranteed. In addition, the
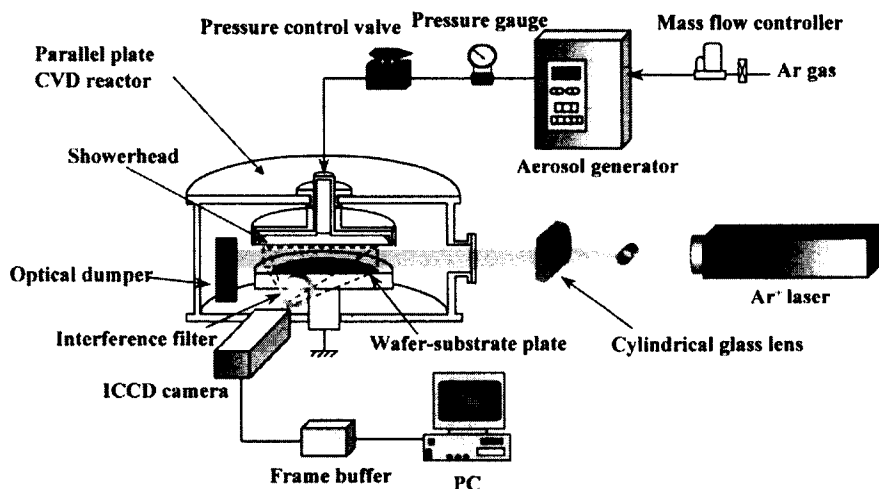
Fig. 1. Schematic diagram of the experimental apparatus and the LLS system used to visualize the particle behavior.

predetermined operating conditions cannot be maintained. Therefore, a pressure reduction system using a pressure control valve was developed to deliver gas–particle mixture from a high-pressure environment to the very low-pressure chamber. This device has been successfully used to study particle behavior in a low-pressure environment.

The volumetric flow rate of the gas in all experiments was set constant at a constant value of 300 sccm by means of a mass flow controller. The operating pressure of the reactor was varied from 2.0 to 4.0 Torr. When thermophoresis effect on the particle transport is not considered, the wafer-substrate plate is not heated. The effect of thermophoresis was investigated by heating the wafer-substrate plate, the temperature of which was set to 300°C. The actual temperature of the plate cannot be represented by a single value since it is difficult to achieve a uniform distribution over the entire surface. Therefore, the temperature distribution was measured using a thermocouple. The temperature distribution of the showerhead and other walls was also measured. The measured and the corresponding fitted lines of the radial profiles of the showerhead and the wafer-substrate plate temperatures are shown in Fig. 2 for a pressure of 2.0 Torr. The same results were obtained for a pressure of 4.0 Torr. The measured wall temperatures were for later use as boundary conditions for numerical simulations.

The spatial distribution of particles was observed by an LLS technique. A laser beam 488 nm in wavelength and approximately 2.0 W in power from an Ar^- laser (Model-2017, Spectra Physics) was expanded to form a light sheet 33 mm in height and 1 mm in thickness using a rod and a cylindrical lens. The laser sheet was passed through a window of the reactor in order to irradiate the space between the plates, from approximately 1 mm below the showerhead and 1 mm above the wafer-substrate plate. An image intensified charged couple device (ICCD) camera (IMAX 512, Princeton Instruments, Inc.) having an
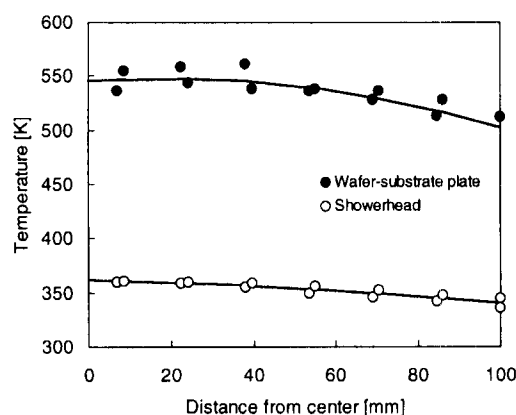

Fig. 2. The measured and the fitted lines for temperature distribution along the radial direction of the showerhead and the wafer-substrate plate. The fitting equations take the form of $T = -1283.0r^2 - 84.658r + 361.79$ for the showerhead and $T = -5678.8r^2 + 189.06r + 547.11$ for the wafer-substrate plate.

interference filter (center wavelength: 488 nm, full-width at half-maximum: 1 nm) was used to detect the light scattered by particles. The signal was passed through a frame buffer and was recorded using a PC.

3. Governing equations and numerical simulation

A numerical simulation was performed using the commercially available CFD code Fluent 5.3 (Fluent, Inc.). The particle trajectories were calculated using a Lagrangian formulation. The individual particle trajectory is tracked by solving the following force balance equations for each particle:

$$\frac{dx_p}{dt} = u_p \qquad (1)$$

and

$$m_p \frac{d\mathbf{u}_p}{dt} = \mathbf{F}_g + \mathbf{F}_D + \mathbf{F}_T, \qquad (2)$$

where $\mathbf{x}_p$ and $\mathbf{u}_p$ are the particle position and velocity, respectively. $\mathbf{F}_g$, $\mathbf{F}_D$ and $\mathbf{F}_T$ are the forces acting on the particle due to gravity, fluid drag and thermophoretic forces, respectively. The drag force is calculated according to Stokes–Cunningham law to account for non-continuum effects at low pressures and is written as

$$\mathbf{F}_D = \frac{3\pi\mu d_p}{C_c}(\mathbf{u} - \mathbf{u}_p). \qquad (3)$$

The Cunningham slip correction factor C_c is given by

$$C_c = 1 + Kn[1.257 + 0.4\exp(-1.1/Kn)]. \qquad (4)$$

Thermophoretic force is calculated based on the equation proposed by Talbot, Cheng, Schefer, and Willis (1980) and is expressed as

$$\mathbf{F}_T = -\frac{6\pi d_p \mu^2 C_s (K + C_t Kn)}{\rho(1 + 3C_m Kn)(1 + 2K + 2C_t Kn)} \frac{1}{T} \nabla T. \qquad (5)$$

In the simulation, it is assumed that the particle is sufficiently dilute so that particle–particle interactions and the effects of the particle volume fraction on the gas phase are negligible. Therefore, the particle trajectories can be calculated based on a fixed gas phase flow field obtained prior to the calculation of particle trajectories.

The set of equations that govern for the gas phase flow are described by continuity, momentum and energy equations for a compressible flow. The compressible flow was used because of the large variations in pressure in the reactor, especially in the showerhead structure. Pressure work and kinetic energy are accounted for in the energy equation of compressible flow model. The gas is assumed to obey the ideal gas law. Viscous dissipation is neglected.

The numerical analysis employed to solve the governing equations is based on the finite volume formulation. The simulations were performed in a full three-dimensional mode to take into account the complicated geometry of the showerhead structure. The computational domain was extended from the inlet tube above the showerhead structure to the exhaust line, which is located at the sidewall as shown in Fig. 3(a). Figs. 3(b) and (c) show the enlarged picture and details of the showerhead structure, respectively. The number, diameter and arrangement of holes at the showerhead and baffle are exactly set the same as real ones. In Fig. 3(a), the boundary conditions used in the simulation are also displayed. The no-slip wall condition is applied to the walls. The fluid mass flux at the inlet is specified using a profile for a fully developed flow through a pipe. A pressure outlet boundary condition is used on the exit boundary in which the gauge pressure is set to zero. For heating conditions, in which the energy equation is solved, the measured wall temperatures shown in Fig. 3(a) were used for both pressure of 2.0 and 4.0 Torr.
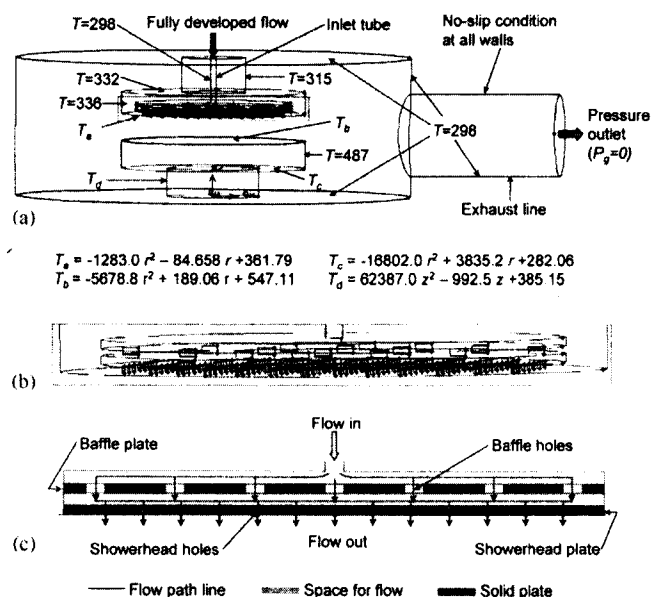

Fig. 3. (a) Computational domain and boundary conditions for the numerical simulation, (b) enlarged picture of the showerhead structure shown in (a), and (c) detail of the showerhead structure. The unit of temperature T shown in this figure is in K. r and z in the fitting equations of temperature profile represent radial and axial positions in m, respectively.

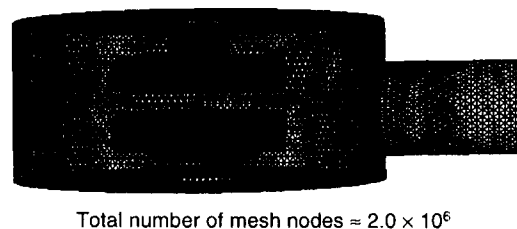Total number of mesh nodes $\approx 2.0 \times 10^6$

Fig. 4. Unstructured triangular/tetrahedral grid arrangement used in the calculation.

The reactor geometry is represented as unstructured triangular/tetrahedral meshes containing approximately 2.0×10^6 nodes. The grid arrangement is shown in Fig. 4. A mesh size of 2.5×10^{-3} m is applied for the inlet tube, the showerhead structure and the space between the plates, and 5.0×10^{-3} m for the other. The solution of momentum and energy equations is approximated by second order upwind differencing scheme in order to minimize numerical diffusion since, in the triangular/tetrahedral grid arrangement, the grid is not aligned with the flow. The pressure–velocity coupling is treated using the Semi-Implicit Method for Pressure Linked Equations (SIMPLE) algorithm of Patankar (1980).

The particle trajectories are calculated by releasing particles with zero momentum from the inlet surface. This initial condition can be justified since the relaxation time, i.e. the time required for particle to adopt the fluid velocity, of 1.0 μm size particle is approximately 6.196×10^{-8} and 6.123×10^{-8} s for pressures of 2.0 and 4.0 Torr, respectively. Assume that argon gas enters the tube with the

volumetric flow rate of 300 sccm. If the flow is assumed to be fully developed, the maximum gas velocity is approximately 125 m/s at the center axis for pressure 2.0 Torr. Thus, the particle will travel along a distance of about 8.0×10^{-6} m to adopt the gas velocity. This distance is much smaller than the length of the inlet tube. Therefore, it would be expected that the particles have adopted the gas velocity before leaving the tube and entering the showerhead structure so that the calculation of particle trajectory inside the reactor will not be affected by this initial condition. When the particles impinge chamber surfaces, they are assumed to be perfectly absorbed.

4. Results and discussion

4.1. Comparisons of particle visualization and simulation

Fig. 5 shows the particle visualization image in the space between the plates with the corresponding trajectory from simulation for different wafer-substrate plate temperatures and pressures. The slopes of trajectory with an arrow in each image of experiment as well as of simulation are plotted in Fig. 6 to compare the measured and simulated trajectory. The figures were taken at a vertical plane that has an angle of 45° to the axis of the exhaust line. All two-dimensional figures presented hereafter will be given at the same position. For each figure of the visualization image, the upper part corresponds to the showerhead and the lower part to the wafer-substrate plate. The left-hand side is the opposite side of the exhaust port and the right-hand side is the region close to the exhaust port. The brighter image in the irradiating plane represents the existence of particles, while the darker regions denote the absence of particles. Since only a vertical sheet of laser light is used to illuminate the particles, the image is only obtained when the particles pass through the light sheet. No information is available regarding the origin of the particles or their fate. Thus, this illumination technique limits measurements to a single cross section of the particles and it is not possible to obtain a complete three-dimensional structure of the particle trajectories. However, the measurement technique provides useful information regarding particle behavior and dynamics in the space between plates. The effect of operating conditions such as temperature and pressure on particle trajectories can be easily investigated.

To reproduce a two-dimensional image of the experiments from a three-dimensional calculation, the following procedure was carried out. The trajectory of approximately 30,000 particles was calculated in order to obtain a representative pattern. From the total number of particles tracked, about 50% were trapped in the showerhead structure. When a particle being tracked passes through a specified plane, the particle position was recorded. The thickness of the plane is 1 mm, the same as that of the laser sheet, which irradiates the space between the plates. A two-dimensional image

of the particles on the plane was then reconstructed. In the simulated particle images, lines that encase an ensemble of particles were added as a visual guide to make the trajectories clearer.

A uniform distribution of particle trajectories can be seen in the simulated images for all operating conditions. This corresponds to the position and the number of the showerhead holes above the top edge of the plane. On the contrary, a uniform distribution cannot be seen in the visualization images. The simulated trajectories were taken in a plane in which the top edge always coincides with a series of showerhead holes that form a line. This differs from the experiments where the top edge of laser sheet does not always coincide with a series of holes that form a line and it may vary from experiment to experiment.

Even though the simulation and the experiment are not precisely the same, however, the same general features can be observed. At ambient temperature, i.e. when the wafer-substrate plate is not heated, the following pattern can be observed both for 2.0 and 4.0 Torr pressure conditions. At the middle part, the particle transport is dominated by the downward direction once the particles enter the reactor through the showerhead holes. At other regions, the particles change their transport direction smoothly. The pattern of the trajectories is similar for 2.0 and 4.0 Torr pressures, suggesting that the particle trajectory is not influenced by the operating pressure for the range of conditions examined herein. This phenomenon was also observed by Nijhawan, McMurry, and Campbell (2000), in that the collection efficiency on the wafer is not influenced by pressure.

When the wafer-substrate plate temperature is set to 300°C, the particle trajectories change significantly from those where no heat was applied, for both 2.0 and 4.0 Torr pressures. A sharp bend can be seen, when the particles approach the wafer-substrate plate. Effect of pressure on particle transport can be observed. The sharper bend is more obvious for a pressure 2.0 Torr as indicated by a more abrupt change in its slope (see Fig. 6). The results show that the experimentally observed phenomena can be satisfactorily reproduced by simulation. The mechanisms of the particle transport will be discussed below.

4.2. Validation of simulations

Before investigating the particle transport mechanisms, it is necessary to verify that the predicted flow field is sufficiently accurate. Since the showerhead structure is the most critical part due to a much smaller length scale compared to the size of the reactor, the pressure drop across the structure was measured in the absence of particles. Fig. 7 shows the measured and the predicted inlet pressure for different chamber pressures ranging from 0.72 to 7.0 Torr. It can be seen that the general trend of the predicted inlet pressure is in good agreement with the measurements.

Experiment   Simulation
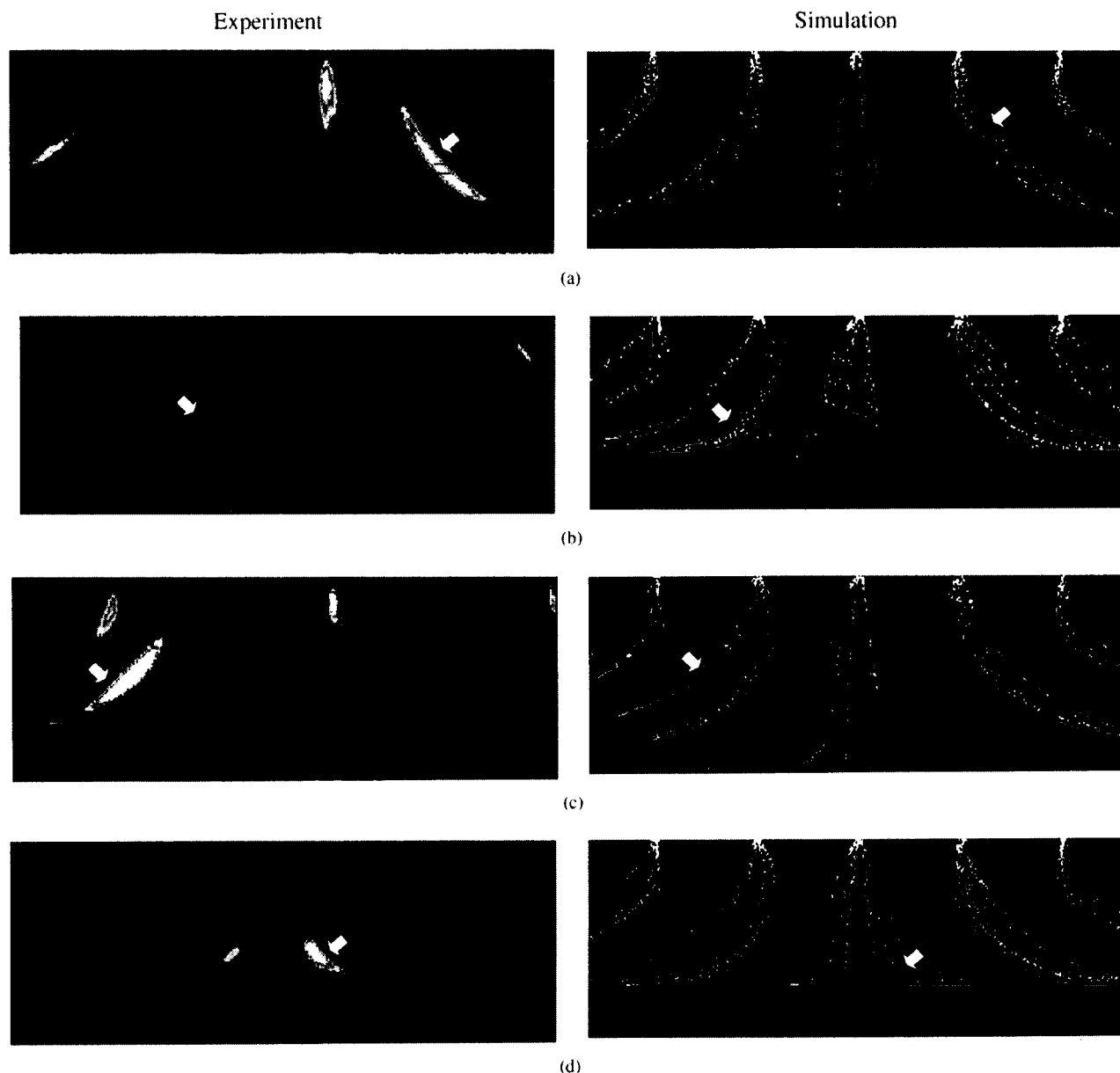

(a)

(b)

(c)

(d)

Fig. 5. Comparison of the visualization and the simulated images for particle trajectories in the space between the plates for various operating conditions: (a) reactor pressure 4.0 Torr without heating, (b) reactor pressure 4.0 Torr with heating by setting the wafer-substrate plate temperature to 300°C, (c) reactor pressure 2.0 Torr without heating, and (d) reactor pressure 2.0 Torr with heating by setting the wafer-substrate plate temperature to 300°C. The slopes of trajectory pointed with an arrow are plotted in Fig. 6.

The predicted inlet pressure increases in an almost linear manner with the chamber pressure where there is a sudden change of slope at pressure 2.0 Torr. This trend is consistent with the measurement. The predicted pressure is slightly lower than that of the measured value, which may be caused by the low-pressure conditions. For low-pressure conditions, the continuum fluid approximation becomes less accurate, since the Knudsen number becomes small, i.e. the gas mean free path becomes more comparable to chamber dimensions, especially in the showerhead structure. In addition, since the reactor geometry has features of disparate

length scales, the accuracy of the overall calculation may be impeded.

4.3. The simulated flow field

Numerically generated steady state flow field in the space between the plates for a pressure of 4.0 Torr for the case of no heating condition (on the left) and pathlines for the case of no heating and heating conditions (on the right) are displayed in Fig. 8. Even though the overall flow patterns inside the entire reactor are quite different for the case of
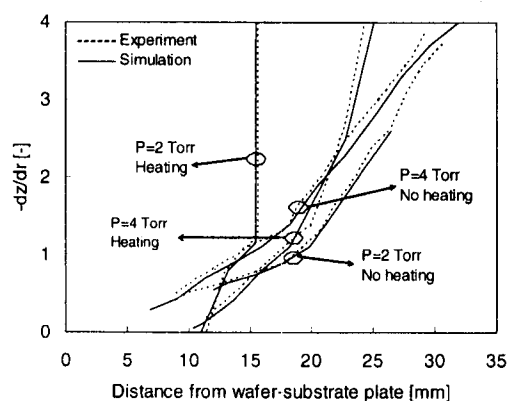
Fig. 6. Change of representative particle trajectory direction in the space between plates as a function of axial distance.
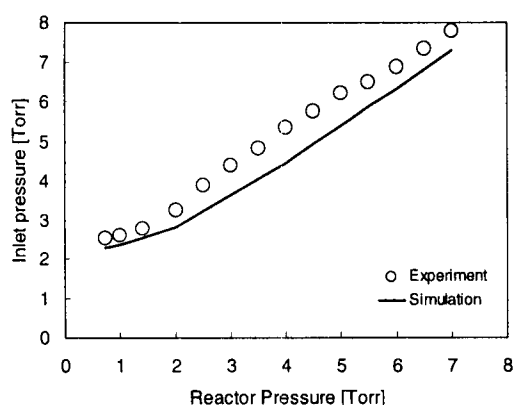

Fig. 7. Comparison of the measured and predicted pressures at the inlet tube for various reactor pressures.
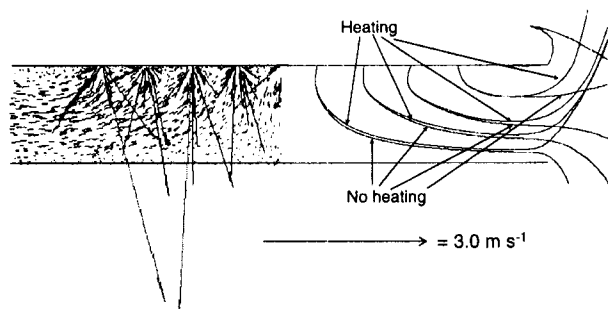

Fig. 8. Simulated gas flow field in the space between the plates for the case of no heating condition (on the left) and pathlines for the case of no heating and heating conditions (on the right). The display of some vectors in the velocity field is omitted to make it clearer. The operating pressure is 4.0 Torr.

no heating and heating conditions, however, the general gas flow patterns in the space between the plates for all conditions examined are similar. It can be seen in Fig. 8 in which the pathlines for no heating condition almost coincide with those of heating conditions. The gas flow enters the space between the plates through the holes of the showerhead, which
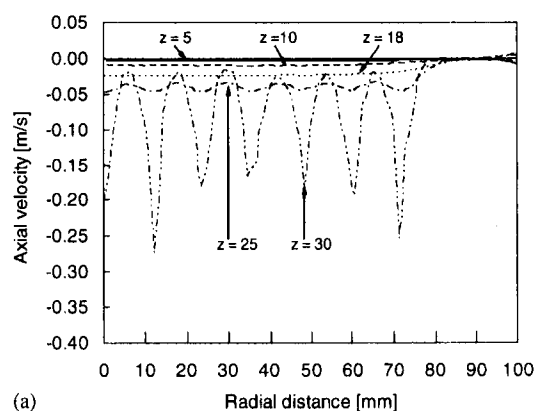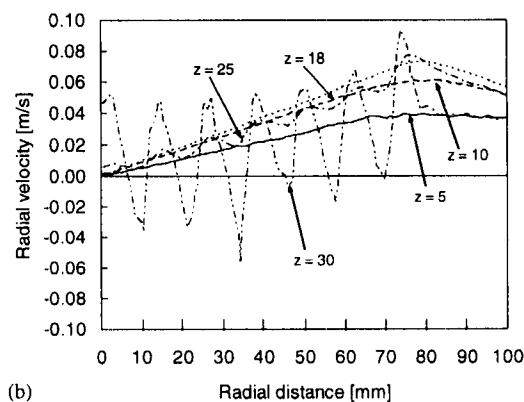
Fig. 9. The velocity profiles along a radial cut at a distance of 5, 10, 18, 25 and 30 mm above the wafer-substrate plate for a pressure of 4.0 Torr and a no heating condition, (a) axial velocity and (b) radial velocity.

accelerates and directs the flow toward the wafer-substrate plate. The velocity decay out so fast once the flow leaves the holes of the showerhead. The flow then bends laterally outward except in the middle region where the dominant velocity direction remains vertically downward. As the flow approaches the wafer-substrate plate, it is deflected at nearly a 90° angle. An area of near stagnation is present in the vicinity of the wafer-substrate plate. For heating conditions, the flow is directed slightly upward when leaving the space between the plates. To clarify this, a radial profile of the axial and radial velocity component at several axial positions in the space between the plates is displayed in Fig. 9 for a pressure 4.0 Torr and no heating condition. At a distance of 30 mm above the wafer-substrate plate (5 mm below the showerhead), the fluctuation in the radial and axial velocities is large. The peak indicates the location of the holes. The radial velocity is nearly zero at the center and then increases along with the radial direction when the effect of the jet diminishes.

4.4. The simulated particle trajectories

A typical illustration of simulated particles trajectories viewed from the bottom is shown in Fig. 10 for a pressure
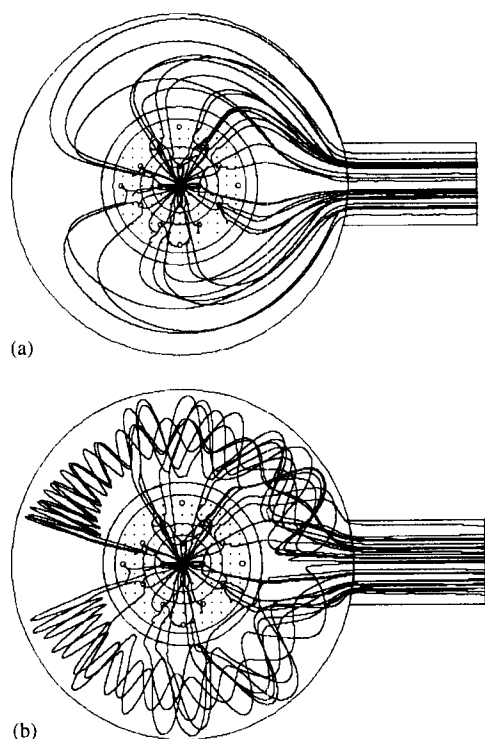
(a)

(b)

Fig. 10. Bottom view of the simulated particle trajectories for pressure 4.0 Torr: (a) no heating condition, and (b) heating condition by setting the wafer-substrate plate temperature to 300°C.
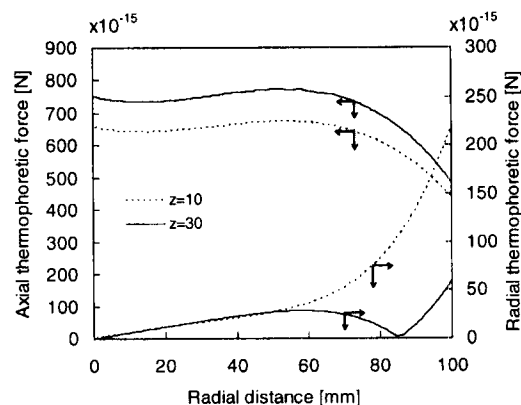

Fig. 11. The axial and radial profiles of the thermophoretic force along a radial cut at a distance of 10 and 30 mm above the wafer-substrate plate for the case of pressure 4.0 Torr and heating conditions by setting the wafer-substrate plate temperature to 300°C.

of 4.0 Torr with the conditions of no heating and heating of the wafer-substrate plate. The particles were initially distributed uniformly on the inlet surface, entering the space between the plates in the reactor through the showerhead and are uniformly distributed in the tangential direction. For no heating conditions, the trajectories are simple. Once the particles exit the space between the plates, they follow the gas flow and proceed directly to the exhaust port. However, when the wafer-substrate plate is heated, the particle trajectories are more complicated. In this case, they travel to the exhaust port in a circulating manner. The flow field for heating conditions outside the space between the plates is quite different from those where no heating is applied. There are extensive circulation flows due to natural convection and the interplay among the forces acting on the particles appears to be complicated.

4.5. The particle transport mechanisms

In this section, the mechanism of particle transport will be examined based on the simulation results. Fig. 11 shows the corresponding axial and radial component of thermophoretic force acting on a particle under the heating conditions at pressure 4.0 Torr. The trend for pressure 2.0 Torr is the same even though the magnitude is higher. The axial thermophoretic force is large at the middle part and then decreases close to the edge of the plates. Compared to gravitational force, the axial component of the

thermophoretic force is on the order of approximately 550 higher. The axial drag force is a decreasing function of the distance from the showerhead. Therefore, when a particle approaches the wafer-substrate plate, the influence of the axial drag force becomes smaller and particle transport is dominated by the thermophoretic force. Consequently, a sharp bend is observed in the particle trajectories when the particles approach the wafer-substrate plate. This differs from the no heating condition due to the lack of thermophoresis. In this case, the particles turn smoothly.

The radial component of the thermophoretic force is smaller than that of the axial component, but it is still larger than the gravitational force. At a distance of 10 mm above the wafer-substrate plate, the force is nearly zero at the center and then increases with radial distance. At the center, the temperature gradient is nearly zero. At a distance of 5 mm below the showerhead, the force fluctuates from zero at the center, gradually increasing to a certain level, then decreasing again, and eventually increases almost linearly. The temperature fluctuation is large in the area close to the showerhead. The gas temperature is lower in the area just below the holes since a lower temperature gas enters the reactor with high velocity. Consequently, there is a large fluctuation on the thermophoretic force.

In order to understand more clearly the effect of thermophoresis on particle transport in the reactor, we characterize the particle deposition to a region between radial distance r_i and r_{i+1} ($i = 1, N$) on the wafer as a non-dimensional particle deposition efficiency. It is defined as the fraction of particles entering the reactor that end up being deposited to the specified region on the wafer. The particle deposition efficiency as a function of radial distance is shown in Fig. 12. When the wafer-substrate plate is heated, there is no particle deposit onto the wafer for both 2.0 and 4.0 Torr pressures. However, when heating is not applied on the plate, particle deposition occurs. The deposition efficiency increases
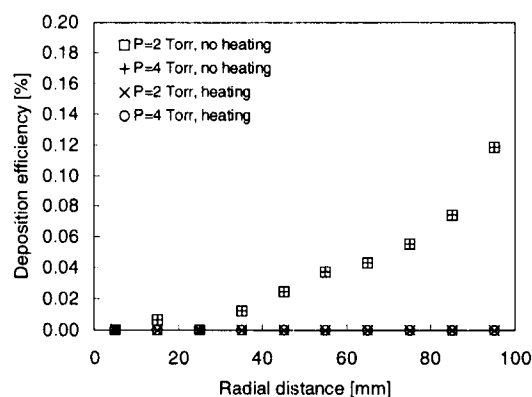
Fig. 12. Calculated deposition efficiency to the wafer-substrate plate as a function of radial distance for various conditions under study.

by increasing the radial distance. The trend is the same for pressures 2.0 and 4.0 Torr.

The effect of thermophoresis on particle trajectory in the space between the plates has been shown. As revealed by the simulation, by heating of the wafer-substrate plate, the flow patterns inside the entire reactor are quite different from those where no heating is applied except in the space between the plates, where a significant difference cannot be observed. This suggests that the change in particle trajectory in the space between the plates by heating of the wafer-substrate plate is primarily caused by thermophoresis. Both numerical and experimental results indicate that the thermophoretic force repels the particles from the wafer-substrate plate. However, it is not the wafer-substrate plate temperature that is important, but, rather, the temperature gradient between the wafer-substrate plate and the showerhead. Therefore, to minimize wafer contamination by minimizing particle deposition onto it the temperature gradient should be increased. Since, for a specific film deposition process, the temperature of the wafer is specific, raising the wafer temperature is nearly impossible. Therefore, the temperature gradient should be increased by reducing the showerhead temperature.

5. Conclusions

It has been demonstrated that the developed system of particle delivery from high pressure environment to low pressure chamber and of particle visualization has been used successfully to investigate particle transport and behavior in a low-pressure parallel plate CVD reactor. The visualization images of particle trajectories in the space between the plates using an LLS technique can be reproduced satisfactorily by a three-dimensional simulation by taking into consideration configuration details of the reactor. As revealed by both experiment and simulation, particle transport in the reactor is not influenced by pressure when the wafer-substrate plate is not heated. This differs from situations where in the

wafer-substrate plate is heated, in which case the particle trajectories are strongly influenced. Simulations reveal that the change of particle trajectories as a result of heating the wafer-substrate plate, is primarily caused by thermophoresis effects.

Notation

C_c	Cunningham correction factor, dimensionless
C_m, C_s, C_t	constants in Eq. (5), dimensionless
d_p	particle diameter, m
F_D	drag force, N
F_g	gravity force, N
F_T	thermophoretic force, N
K	ratio of the gas and particle thermal conductivities, dimensionless
Kn	Knudsen number, dimensionless
m_p	particle mass, kg
t	time, s
T	temperature, K
u	gas velocity, m/s
u_p	particle velocity, m/s
x_p	particle position, m

Greek letters

μ	gas viscosity, kg/m s
ρ	gas density, kg/m^3

Acknowledgements

References

Adachi, M., & Okuyama, K. (1998). Particle deposition in air. in: Hattori (ed.), *Ultraclean surface processing of silicon wafers: Secrets of VLSI manufacturing* (pp. 67–81). Berlin: Springer.

Choi, S. J., Rader, D. J., & Geller, A. S. (1996). Massively parallel simulations of Brownian dynamics particle transport in low pressure parallel-plate reactor. *Journal of Vacuum Science and Technology A, 14*(2), 660–665.

Collins, S. M., Brown, D. A., O'Hanlon, J. F., & Charlie, R. N. (1995). Postplasma particle dynamics in a gaseous electronic conference RF reference cell. *Journal of Vacuum Science and Technology A, 13*(6), 2950–2953.

Fujimoto, T., Okuyama, K., Shimada, M., Fujishige, Y., Adachi, M., & Matsui, I. (2000). Particle generation and thin film surface morphology in the tetraethylorthosilicate/oxygen plasma enhanced chemical vapor deposition process. *Journal of Applied Physics, 88*(5), 3047–3052.

Garrity, M. P., Peterson, T. W., Garret, L. M., & O'Hanlon, J. F. (1995). Fluid simulations of particle contamination in postplasma processes. *Journal of Vacuum Science and Technology A, 13*(6), 2939–2944.

MacGibbon, B. S., Busnaina, A. A., & Fardi, B. (1999). The effect of thermophoresis on particle deposition in a tungsten low pressure chemical vapor deposition reactor. *Journal of The Electrochemical Society, 146*(8), 2901–2905.

Nijhawan, S., McMurry, P. H., & Campbell, S. A. (2000). Particle transport in a parallel-plate semiconductor reactor: Chamber modification and design criterion for enhanced process cleanliness. *Journal of Vacuum Science and Technology A, 18*(5), 2198–2206.

Oh, M. D., Yoo, K. H., & Myong, H. K. (1996). Numerical analysis of particle deposition onto horizontal freestanding wafer surfaces heated or cooled. *Aerosol Science and Technology, 25*, 141–156.

Okuyama, K., Huang, D. D., Seinfeld, J. H., Tani, N., & Kousaka, Y. (1991). Aerosol formation by rapid nucleation in the preparation of SiO$_2$ thin film from SiCl$_2$ and O$_2$ gases using CVD process. *Chemical Engineering Science, 46*(7), 1545–1560.

Okuyama, K., Huang, D. D., Seinfeld, J. H., Tani, N., & Matsui, I. (1992). Gas-phase nucleation in GaAs thin film preparation by MOCVD. *Japanese Journal of Applied Physics, 31*(1), 1–11.

Patankar, S. V. (1980). *Numerical heat transfer and fluid flow*. London: Taylor & Francis.

Rao, N. P., Wu, Z., Nijhawan, S., Ziemann, P., Campbell, S., Kittelson, D. B., & McMurry, P. (1998). Investigation of particle formation during the plasma enhanced chemical vapor deposition of amorphous silicon, oxide, and nitride films. *Journal of Vacuum Science and Technology B, 16*(2), 483–489.

Schmidt, F., Fissan, H., & Schmidt, K. G. (1996). Transport of submicron particles from a leak to a perpendicular surface in a chamber at reduced pressure. *Journal of Aerosol Science, 27*(5), 739–750.

Slater, S. A., & Young, J. B. (2001). The calculation of inertial particle transport in dilute gas–particle flows. *International Journal of Multiphase Flow, 27*, 61–87.

Talbot, L., Cheng, R. K., Schefer, R. W., & Willis, D. R. (1980). Thermophoresis of particles in a heated boundary layer. *Journal of Fluid Mechanics, 101*(4), 737–758.

Ye, Y., Pui, D. Y. H., Liu, B. Y. H., Opiolka, S., Blumhorst, S., & Fissan, H. (1991). Thermophoretic effect of particle deposition on a free standing semiconductor wafer in a clean room. *Journal of Aerosol Science, 22*(1), 63–72.